PHILOSOPHICAL TRANSACTIONS OF THE ROYAL SOCIETY A MATHEMATICAL, PHYSICAL & ENGINEERING SCIENCES

Air entrainment upon liquid impact

A. Prosperetti and H. N. Oguz

Phil. Trans. R. Soc. Lond. A 1997 **355**, 491-506
doi: 10.1098/rsta.1997.0020

Air entrainment upon liquid impact

By A. Prosperetti and H. N. Oğuz

Department of Mechanical Engineering, The Johns Hopkins University, Baltimore, MD 21218, USA

The impact of round and plane liquid jets on plane liquid surfaces is simulated numerically on the basis of a potential flow model. It is found that the mass of the jet is as important as its momentum in determining the flow. For sufficiently long jets and small Froude numbers air cavities are entrained. Entrainment is more unlikely in two dimensions than in three.

1. Introduction

The *Acts of the Apostles* informs us that a 'stone fallen from the sky'† was worshipped in the famed Temple of Artemis in Ephesus, one of the Seven Wonders of the ancient world. This is one of the earliest references to a natural process that falls under the purview of the present volume, *Violent Surface Motion*. With typical impact velocities of 1–20 km s^{-1}, one can estimate impact pressures in the range of tens to thousands of kbars, which are large enough to cause fluid-like flow of the solid material involved in the impact (see, for example, O'Keefe & Ahrens 1986). Interesting as such extreme events might be, in the present paper we tackle considerably more modest problems in which the 'violence' is taken to refer to the fact that, at least during part of the process, the temporal contribution to the fluid particle acceleration is considerably greater than the convective one.

The practical importance of fluid motions of this type has numerous and diverse aspects that include, for example, the slamming of floating bodies on the ocean surface as well as cavitation damage. Our own interest is motivated by their occurrence in air entrainment processes.

The entrapment of bubbles in a liquid is such an ordinary experience that the gurgling sound they produce is commonly identified—often mistakenly—with the sound of flowing water itself. But aside from its common occurrence, there are many practical reasons that make this process worth studying. For example, air entrainment can be detrimental in industrial operations such as the pouring of molten metals and plastics, or beneficial in situations such as the aeration of liquids, from the ocean to fish-farm ponds.

In spite of their importance and widespread occurrence, the study of air entraining flows is relatively little developed. In considering the reasons for this situation, one may point out that, in the first place, the formation and breaking off of a bubble is such an extreme modification of the topology of a free surface that linear methods of investigation are of little use. The only sufficiently powerful nonlinear technique—the hodograph transformation (Birkhoff & Zarantonello 1957; Milne–Thomson 1960;

† King James version, 19:35; the Greek original is actually less specific.

Phil. Trans. R. Soc. Lond. A (1997) **355**, 491–506
Printed in Great Britain

Gilbarg 1960)—is exclusively available for two-dimensional flows and, even in that case, it has a difficult time dealing with time dependence, gravity, and surface tension, all of which play an essential role in the process. This leaves computation, which is, however, plagued by numerical as well as modelling difficulties. On the experimental side, observation is hampered by the extreme rapidity of the cavity closure, the complexity of the flow, the fact that newly formed bubbles impede a clear view of the process by which the following ones are formed, and other difficulties. Furthermore, there are a number of different processes by which air is entrained depending on viscosity, level of surface disturbances, flow rate, geometry, and others (see, for example, the recent review by Biń (1993)).

In the present paper we shall address what seems to be the simplest elementary process, namely the flow that is established when a liquid mass impacts an extended, initially plane, liquid surface. Typical examples would be rain drops or splashes hitting the ocean surface. Less obvious occurrences of such phenomena are some nominally steady situations such as air entrainment by a steady jet falling into a liquid pool. Indeed, for low-viscosity liquids, a close inspection of this situation reveals that air is entrained when disturbances on the surface of the falling jet reach the surface of the pool liquid (Lin & Donnelly 1966; Sene 1988; Oğuz *et al.* 1992; Oğuz & Prosperetti 1994).

2. Overpressure

In view of the complexity of these flows, it is of interest to inquire to what extent the process can be simplified without compromising its fundamental physics. In this spirit we consider the flow established by an overpressure ΔP, constant in time, acting over a given portion A of the surface of an initially quiescent fluid. This might be thought of as representing the transient flow induced by a liquid jet of cross section A impacting normally a plane liquid surface with velocity

$$U = \sqrt{2\Delta P/\rho}. \tag{2.1}$$

We assume the overpressure to act over a surface area πa^2 in three dimensions (cylindrical 'jet'), or over an infinite strip of width $2a$ in two (plane 'jet'). The parameters governing the problem can then be grouped into the Froude, Weber and Reynolds numbers defined, respectively, by

$$Fr = U^2/ag, \quad We = \rho U^2 a/\sigma, \quad Re = aU/\nu. \tag{2.2}$$

Here g is the acceleration due to gravity, σ the surface tension coefficient and ν the kinematic viscosity. Since for most of the applications of interest here the flow is highly transient and the Reynolds number large, we shall neglect viscous effects. For simplicity, we shall also neglect surface tension that is likely to be unimportant except for small drops. Weber number effects on some flows of the general type studied here were considered in some earlier papers (Oğuz & Prosperetti 1990, 1994).

With these assumptions, we can introduce a velocity potential ϕ which solves the Laplace equation subject to the boundary conditions

$$\frac{\partial \phi}{\partial t} + \frac{1}{2}\left|\nabla\phi\right|^2 + \frac{1}{Fr}\eta = p, \tag{2.3}$$

$$\frac{\mathrm{d}\boldsymbol{x}_s}{\mathrm{d}t} = \nabla\phi|_{\boldsymbol{x}_s}. \tag{2.4}$$

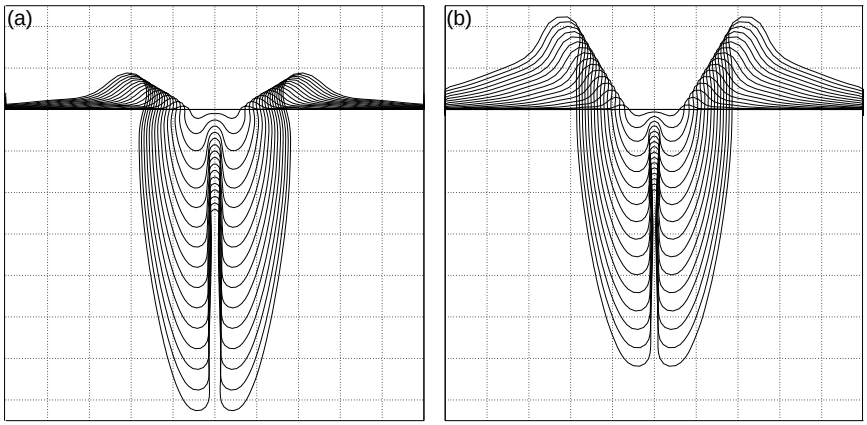

Figure 1. Successive free surface shapes produced by a constant, steady overpressure acting on the surface of a liquid in three (*a*) and two spatial dimensions (*b*) with an infinite Froude number. Successive contours are separated by one dimensionless time unit. The dashed squares have sides equal to two dimensionless units. The overpressure acts over a distance of two units at the center of the figures.

In the expression (2.3) of the dynamic boundary condition, η is the elevation of the free surface above the initial, plane quiescent state and p is the pressure in excess of the undisturbed level non-dimensionalized by ΔP. In the kinematic condition (2.4), $\boldsymbol{x}_s$ is the generic surface point.

These equations have been written in dimensionless form non-dimensionalizing lengths in terms of the jet radius, or half width, a, and velocities in terms of U. The initial conditions are

$$\phi = 0, \quad \eta = 0. \tag{2.5}$$

The problem is solved numerically by a version of the boundary integral method that we have extensively used and documented in our previous papers (see, for example, Oğuz & Prosperetti 1990, 1991, 1993, 1994) to which the reader is referred for details.

We consider a 'top hat' overpressure distribution, $p = 1$ for $0 \leqslant r \leqslant 1$, or $0 \leqslant |x| \leqslant 1$, and $p = 0$ elsewhere. The simplest case is that of $Fr \to \infty$, which is the one we consider first. A sequence of free surface shapes for the axisymmetric and two-dimensional cases is shown in figure 1, left and right, respectively. Here, successive contours are separated by one dimensionless time unit. The squares have sides equal to two dimensionless units. Remarkably, if these profiles are translated so as to align their lowest points, the cavity shapes are found to be very similar in the two geometries. Note the thin column of fluid on the axis, or plane, of symmetry left behind by the advancing cavity. Since the overpressure is prescribed to be uniform, aside from transient effects that may be expected to decrease with time, the modulus of the fluid velocity must be constant. This circumstance prevents the formation of a stagnation point relative to the cavity bottom. It may also be expected that the rate of penetration of the cavity be very nearly $\sqrt{2\Delta P/\rho}$, which is indeed confirmed by the numerical calculation. The only major difference between the two geometries is the bigger splash in the plane case, which may be simply attributed to mass conservation and geometry.

Some examples for finite Froude numbers are shown in figures 2 and 3 in three

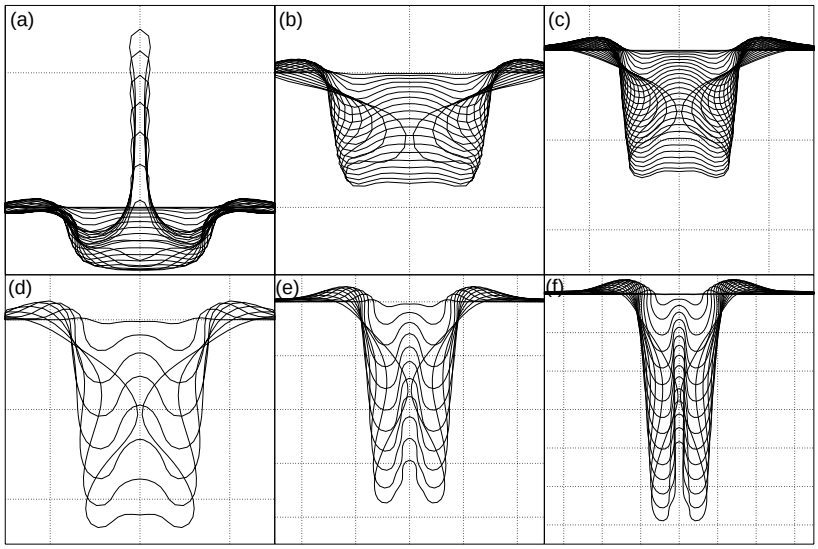

Figure 2. Successive free surface shapes produced by a constant, steady, axisymmetric overpressure acting on the surface of a liquid in the region $0 \leqslant r \leqslant 1$. In the upper row $Fr = 1$, 2, 4. Successive contours are separated by 0.2 dimensionless time units. The last contours shown are, from the left, at times 5, 3.8 and 5.25. In the second row $Fr = 8$, 16, 32. Successive contours are separated by 1 dimensionless time unit. The last contours shown are at times 7.31, 10.5 and 15.2. In all cases the dashed squares sides equal two dimensionless units.

and two dimensions, respectively. Here, from left to right, $Fr = 1, 2, 4$ in the upper row and $Fr = 8, 16$, and 32 in the bottom one. The behaviour for $Fr = 1$ is markedly different from the other cases particularly in the axisymmetric geometry.

Initially the surface disturbance creates a cavity that, because of inertia, overshoots equilibrium and fills up from the bottom with a thin jet. It is likely that a nonlinear oscillatory motion would be found if the calculation were continued past this point. This is indeed the result in the first two-dimensional example of figure 3. With weaker gravity effects, however, the crater collapses inward from the sides before the downward motion of its bottom can be reversed and a large bubble is entrapped, the later the larger Fr.

In figure 4 the circles mark the dimensionless volume V/a^3 of the entrapped bubble in the axisymmetric case and in figure 5 the closing time of the cavity, both as functions of Fr. The corresponding results for the two-dimensional geometry are indicated by squares. The trends displayed in these figures appear to be remarkably simple and it is tempting to try to reproduce them on the basis of scaling arguments.

Consider the axisymmetric case first. One may expect that, if the overpressure is sufficiently large, to a first approximation its precise distribution over the cross sectional area would be immaterial so that the only fundamental parameter would be the surface 'force'

$$\mathcal{F}_3 = \frac{1}{\rho}\int_A \mathrm{d}A\,\Delta P = \pi a^2 \frac{\Delta P}{\rho}, \tag{2.6}$$

where the last step follows from the assumed spatial uniformity of ΔP in the present case. Dimensionally, $[\mathcal{F}_3] = \mathrm{L}^4\mathrm{T}^{-2}$, where L and T are units of length and time. If the only other quantity determining the cavity volume V is gravity, dimensional

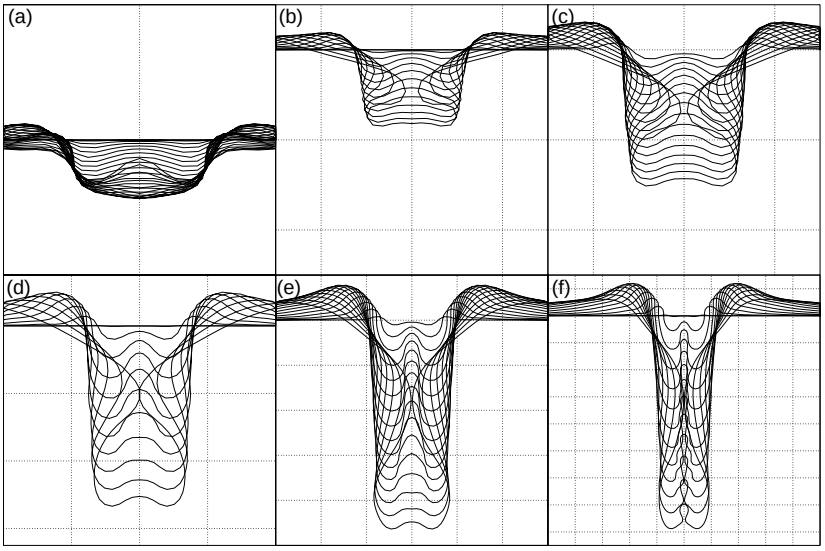

Figure 3. Successive free surface shapes produced by a constant steady two-dimensional overpressure acting on the surface of a liquid in the region $0 \leqslant |x| \leqslant 1$. In the upper row $Fr = 1$, 2, 4. Successive contours are separated by 0.2 dimensionless time units in the first example and by 0.4 in the other two. The last contours shown are, from the left, at times 5, 4.9 and 6.8. In the second row $Fr = 8$, 16, 32. Successive contours are separated by 1, 1 and 2 dimensionless time units. The last contours shown are at times 10.2, 15.6 and 24.4. In all cases the dashed squares sides equal two dimensionless units.

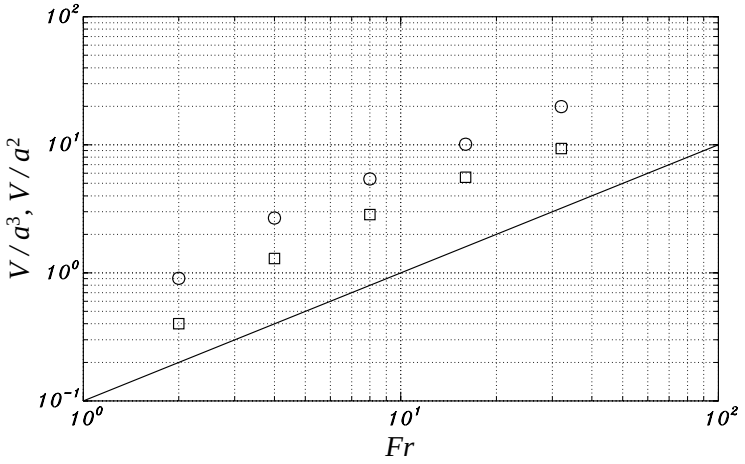

Figure 4. Dimensionless volume of the entrapped bubble with axial symmetry (circles) and in two dimensions (squares) for a constant applied overpressure as a function of the Froude number. The solid line has unit slope. A best-fit to the numerical data gives slopes of 1.067 and 1.087 for three and two dimensions, respectively.

analysis leads us to expect a relation of the type

$$V \propto \mathcal{F}_3/g. \tag{2.7}$$

Upon using the expression (2.6) for $\mathcal{F}_3$ and rewriting this relation in terms of the

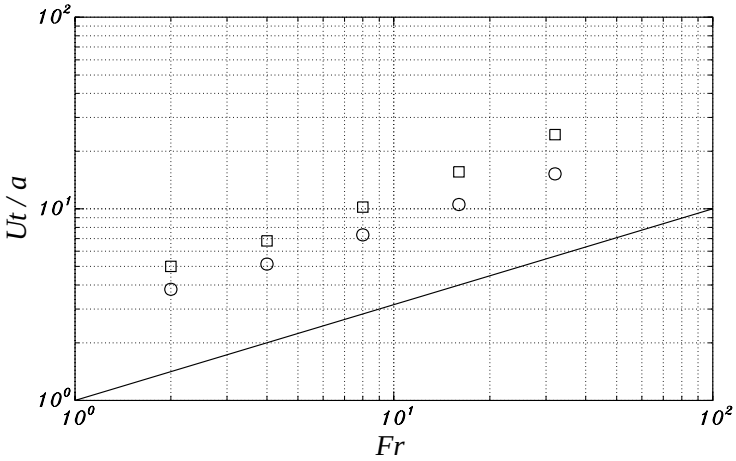

Figure 5. Dimensionless time necessary to entrap a bubble with axial symmetry (circles) and in two dimensions (squares) for a constant applied overpressure as a function of the Froude number. The solid line has slope 1/2. A best-fit to the numerical data gives slopes of 0.506 and 0.584 for three and two dimensions, respectively.

Froude number defined in (2.2), we find

$$V/a^3 \propto Fr\,. \tag{2.8}$$

The solid line in figure 4 depicts this relation and is seen to fit the numerical results remarkably well.

A similar line of reasoning can be followed for the closure time t_c shown in figure 5 to find

$$t_c \propto (\mathcal{F}_3/g^4)^{1/6}, \tag{2.9}$$

from which

$$Ut_c/a \propto Fr^{2/3}\,. \tag{2.10}$$

The solid line in figure 5, which is seen to fit the data very well, is proportional to $Fr^{1/2}$ rather than $Fr^{2/3}$. The scaling (2.10) does not therefore seem to capture the physics of the closure process.

One may explore a different scaling based on the characteristic time for the filling of the crater under the action of gravity, $\sqrt{a/g}$. In this case one finds

$$Ut_c/a \propto Fr^{1/2}, \tag{2.11}$$

which agrees very well with the numerical results. The entrained volume, however, turns out to be proportional to $Fr^{3/4}$, which is at variance with the results of figure 4.

For the two-dimensional case, we are led to use, in place of (2.6),

$$\mathcal{F}_2 = \frac{1}{\rho}\int_{-a}^{a} \mathrm{d}x\,\Delta P = 2a\frac{\Delta P}{\rho}. \tag{2.12}$$

The results corresponding to (2.7) and (2.9) are now

$$V \propto \mathcal{F}_2/g, \quad t_c \propto (\mathcal{F}_2/g^3)^{1/4}, \tag{2.13}$$

from which one finds $V/a^2 \propto Fr$ as in (2.8), and again (2.10) for t_c. The line in figure 4 shows a good agreement with the computed volume. As noted before,

however, the line in figure 5 for the computed closure time has a slope $\frac{1}{2}$ rather than $\frac{2}{3}$. The alternative scaling in terms of $\mathcal{F}_2$ and $\sqrt{a/g}$ gives again $V/a^2 \propto Fr^{2/3}$ and the same scaling (2.11) for t_c. Thus we conclude that, in two, as well as in three, dimensions, a single scaling fails to account for both V and t_c. The volume is seen to respond to the input energy, while the closure time appears to be determined by the kinematics of uniformly accelerated motion.

The previous results have been obtained with an overpressure lasting as long as the cavity closes. If the overpressure duration is too short, one finds that no closed cavity forms similarly to the situation of the $Fr = 1$ cases in figures 2 and 3.

The approach taken in this section was motivated by the desire to simplify the simulation of a liquid jet impacting a liquid surface. To the extent that we have accounted for the momentum of the jet, neglecting its mass, these results may perhaps be better considered as simulations of 'blowing' over the free surface. We now turn to a more realistic simulation of jet impact, including the jet itself, to examine the mass effects.

3. Impacting jet

The formulation of the problem is the same as that given in (2.3) and (2.4). The only difference concerns the initial conditions (2.5). We assume that, at $t = 0$, a column of liquid of unit radius (or, in two dimensions, half-width) impacts the undisturbed surface with unit velocity. The column's dimensionless height h (i.e. its aspect ratio) is kept as a parameter, and the initial value of the potential is

$$\phi(\boldsymbol{x}, t) = z, \quad \text{for} \quad 0 \leqslant z, \tag{3.1}$$

while $\phi = 0$ for $z \leqslant 0$. The dimensionless numbers are defined by the same relations (2.2) as before, in which now U is the velocity of impact. To avoid sharp corners on the free surface, we cap the column with a hemisphere (or semicircle), which is not included in the stated values of the aspect ratio. We have satisfied ourselves that the details of how the column is terminated are immaterial for the development of the flow.

As before, we begin with the infinite Froude number case. Successive free surface configurations are shown in figure 6 for the axisymmetric (left) and plane cases. The jet aspect ratio is $h = 15$. Successive profiles are separated by four time units and the squares have sides equal to five units. Contrary to the overpressure calculation, the crater is seen to expand sideways as its bottom becomes deeper. This effect is due to the need to provide a radial pressure gradient to change the flow direction of the deflected jet liquid that 'coats' the cavity's outer surface, and is therefore a direct consequence of the mass effect mentioned before. Since, due to geometrical effects, the thickness of this coating layer is less in the axisymmetric case, the pressure gradient is correspondingly smaller and the crater narrower.

It is a classic result, in both two and three dimensions, that the rate of penetration of the jet into the receiving liquid is $\frac{1}{2}U$ (Birkhoff *et al.* 1948; Birkhoff & Zarantonello 1957, p. 15). This result depends on the assumption of steady flow and the neglect of splash effects and is therefore valid in the asymptotic limit of large times and deep cavities. The argument is very simple and is as follows. If V is the downward velocity of the frame of reference in which the cavity bottom is at rest, the velocity along the jet surface would be $U - V$, while the velocity along the outer cavity surface

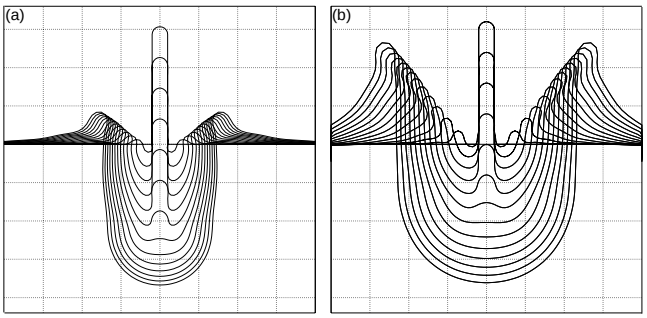

Figure 6. Successive free surface configurations due to the impact of a round (a) and two-dimensional (b) jet with aspect ratio 15. The Froude number is infinite. Successive profiles are separated by 4 time units. The squares have sides of 5 units. The last shape shown is for $t = 52$.

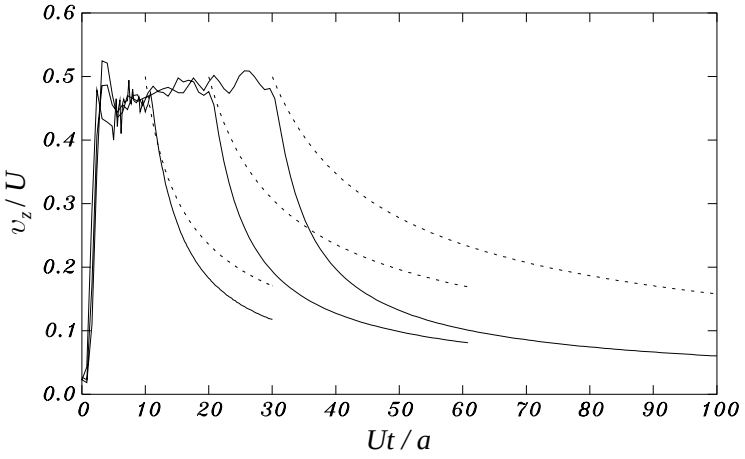

Figure 7. Downward velocity of the cavity bottom for the axisymmetric case with $Fr \to \infty$ and $h = 5$, 10 and 15. The dashed lines are the estimate (3.3).

would asymptotically be V. Since the modulus of the velocity along a steady free streamline must be constant, $U - V = V$ and the result quoted follows.

To test this prediction, we show in figure 7 the computed downward velocity of the axisymmetric cavity bottom as a function of time for $h = 5$, 10, and 15. Aside from some numerical noise, a value close to the asymptotic estimate of 1/2 is attained very quickly, after a depth of penetration equal to about one jet radius. Since the relative velocity of the tail end of the jet with respect to the cavity bottom is $U - \frac{1}{2}U$, complete penetration is expected to occur after a time $t_p = 2h/U$ which, for the cases shown in this figure, equals 10, 20, and 30. This expectation is also well borne out by the figure. Around $t = t_p$, the time dependence of the velocity undergoes a marked change as the motion transitions from an expansion driven by the incoming jet to an inertial regime driven by the accumulated kinetic energy. One can approximate this latter phase assuming conservation of energy for an expanding sphere with radius equal to the depth of the crater $H(t)$:

$$H^3 \dot{H}^2 = h^3 (\tfrac{1}{2}U)^2. \tag{3.2}$$

This expression assumes that, when the inertial stage of the motion begins, the

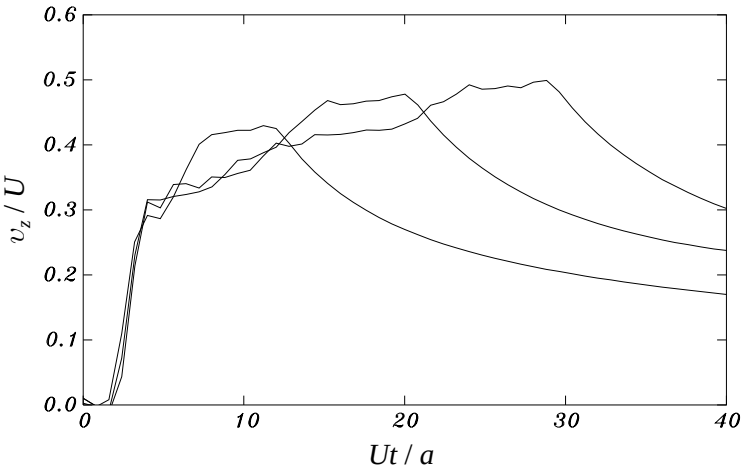

Figure 8. Downward velocity of the cavity bottom for the two-dimensional case with $Fr \to \infty$ and $h = 5$, 10 and 15.

crater has a depth h (which is also a classic result which readily follows from the previous arguments) and a velocity $(\frac{1}{2}U)$. Upon integrating (3.2) subject to $H = h$ at $t_\mathrm{p} = 2h/U$ we find

$$H = h(\tfrac{5}{4}(Ut/h) - \tfrac{3}{2})^{2/5}. \tag{3.3}$$

This relation is shown by the dashed lines in figure 7. It is seen to match fairly well the velocity at the beginning of the inertial expansion, but to overestimate it at later times. This difference is probably the consequence of the fact that (3.2) does not account for the portion of kinetic energy that is taken up by the splash. What remains available for the expansion of the cavity is therefore somewhat less than assumed in (3.2), and therefore the velocity decrease more rapid.

The results of figure 7 show some numerical noise in the early, nearly constant-velocity penetration phase. The quantity plotted is the downward velocity of the lowest point of the cavity, a position that, due to small numerical errors, fluctuates among a few neighbouring nodes. After complete penetration, the cavity lowest node does not change, which accounts for the much smoother portion of the curve for $t > t_\mathrm{p}$.

The two-dimensional case can be considered along the same lines. Figure 8 is a graph of the velocity of the bottom of the cavity versus time. We see that, here, the approach to the asymptotic value is much slower and, as a matter of fact, has barely been completed by the time the jet has been entirely consumed. In this case a model in which the cavity expands as a semi-circle is wrong in principle as the kinetic energy of such a motion would be logarithmically divergent. Thus, the free surface is essential in determining the cavity motion in the two-dimensional case. This is another angle from which the very prominent role played by the splash in this geometry can be viewed.

An exact analytical solution exists for the two-dimensional problem (see, for example, Birkhoff & Caywood 1949; Birkhoff & Zarantonello 1957, p. 36) in the asymptotic limit $t \to \infty$ in which the crater has infinite depth and is given by

$$\frac{z + \mathrm{i}x}{\pi a} = -\frac{4}{(\zeta+1)^2} - \frac{4}{\zeta+1} + 2\log\frac{\zeta+1}{\zeta-1} + 8 + 2\pi\mathrm{i}, \quad \zeta = \exp\mathrm{i}\theta, \quad 0 \leqslant \theta \leqslant \pi. \tag{3.4}$$

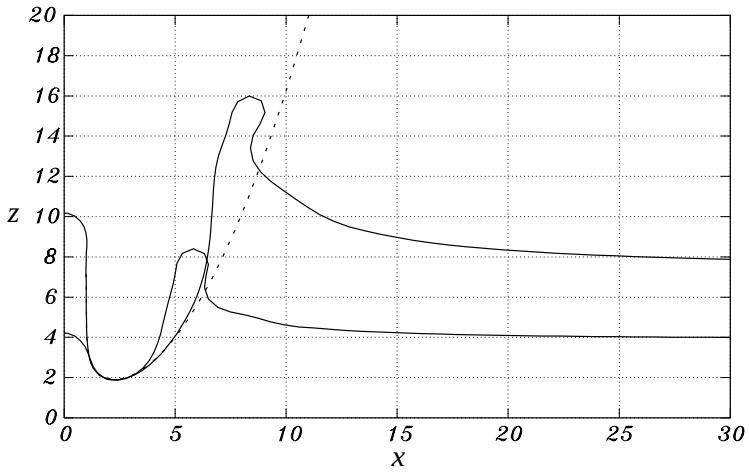

Figure 9. Comparison of the free surface shape with the asymptotic analytic result (3.4) (dashed line) at times 10 and 20 for $h = 15$ and $Fr \to \infty$. The computed surface shapes have been translated downward by 8.4 and 4.2, respectively, so as to match the lowest point of the cavity.

For future reference we note that, far from the cavity bottom, this relation gives

$$x \simeq 4\sqrt{(z/\pi)}. \tag{3.5}$$

We compare the result (3.4) (dashed line) with the computed free surface shape at (dimensionless) times 10 and 20 in figure 9 for $h = 15$. It can be seen that the latter shape follows the asymptotic result over a greater portion of the free surface, as expected. The major difference between the asymptotic and transient solutions is the thick splash thrown upward from the free surface.

We conclude that, in two dimensions, the asymptotic limit (3.4) of an infinitely deep crater is approached very slowly and is therefore only relevant for very long jets. As a consequence, frustratingly long computational times are required to reach 'asymptopia'.

Switching on gravity changes the situation in two major respects, one obvious and the other one perhaps less so. The former is the tendency for the side walls of the cavity to collapse inward, much in the same way as found before in the overpressure case. The second difference is that the velocity of the falling mass keeps increasing as potential energy is traded for kinetic energy. In order to account in an approximate manner for this latter effect, we introduce the modified velocity

$$U_{\mathrm{e}} = \sqrt{U^2 + \tfrac{1}{2}gh}, \tag{3.6}$$

obtained by converting the kinetic plus potential energy of the jet at the moment of initial impact with velocity U to kinetic energy with velocity U_{e}. Correspondingly, we define a modified Froude number by

$$Fr_{\mathrm{e}} = \frac{U_{\mathrm{e}}^2}{ga} = Fr + \frac{1}{2}\frac{h}{a}. \tag{3.7}$$

For jets with a large aspect ratio, the difference between the Froude number at impact, Fr, and the energy-based Froude number, Fr_{e}, can be considerable.

Some results for $Fr = 2$, 8, and 32 are shown in figure 10 for aspect ratios of

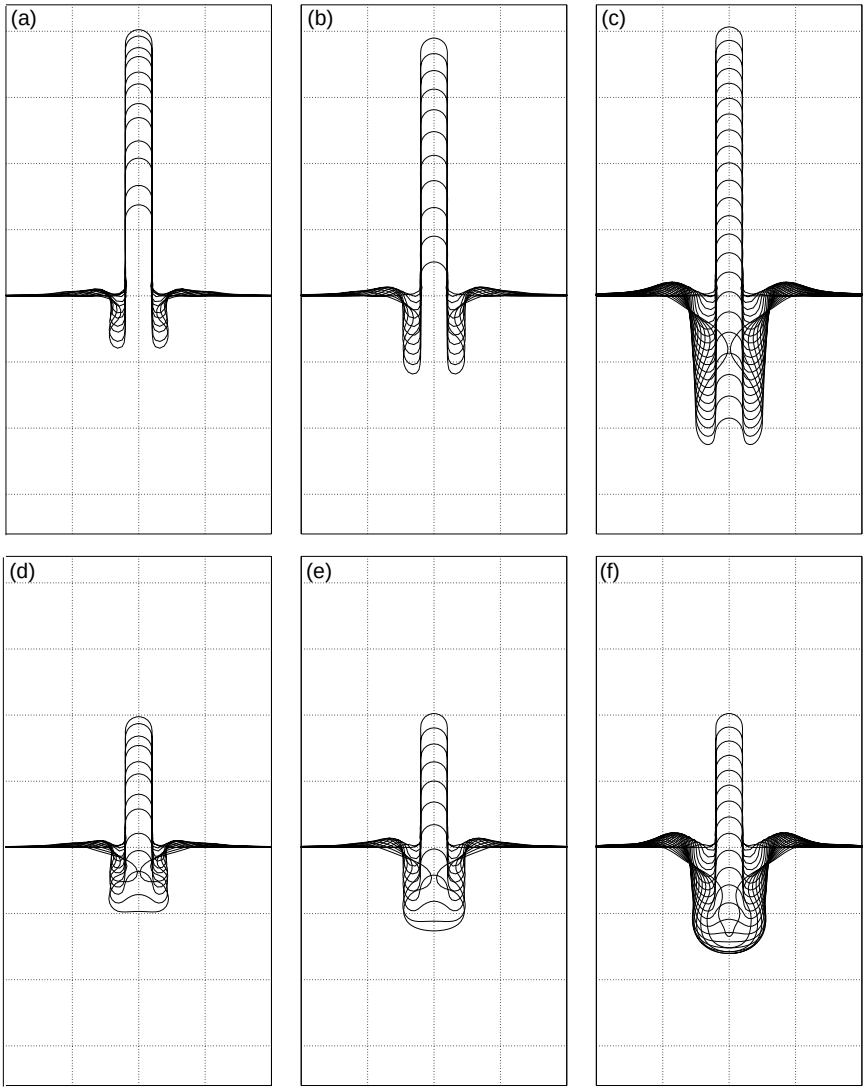

Figure 10. Successive free surface configurations due to the impact of a round jet with aspect ratio 20 (top row) and 10. The Froude number equals 2 for (a) and (d), 8 for (b) and (e) and 32 for (c) and (f). Successive contours are separated by 0.5 dimensionless time units in (a) and (d) and by 1 unit in the other cases. The last contours shown are, in alphabetical order, at times 5.9, 10.7, 22, 6.2, 11.2 and 22.2. In all cases the dashed squares sides equal 5 dimensionless units.

20 and 10. In the former case, with increasing Fr, there is a transition between a situation in which the cavity walls collapse against the jet and one in which the jet has penetrated below the closure point by the time closure takes place. The volume of entrapped air is significantly different in the two regimes. For the shorter jet, the first regime is not observed in the range of Froude numbers shown, but a further qualitative different phenomenon begins to appear for $Fr = 32$, figure 10f. After the jet has been consumed, the downward motion of the cavity bottom starts decreasing and eventually reverses. At slightly higher Froude numbers, this process

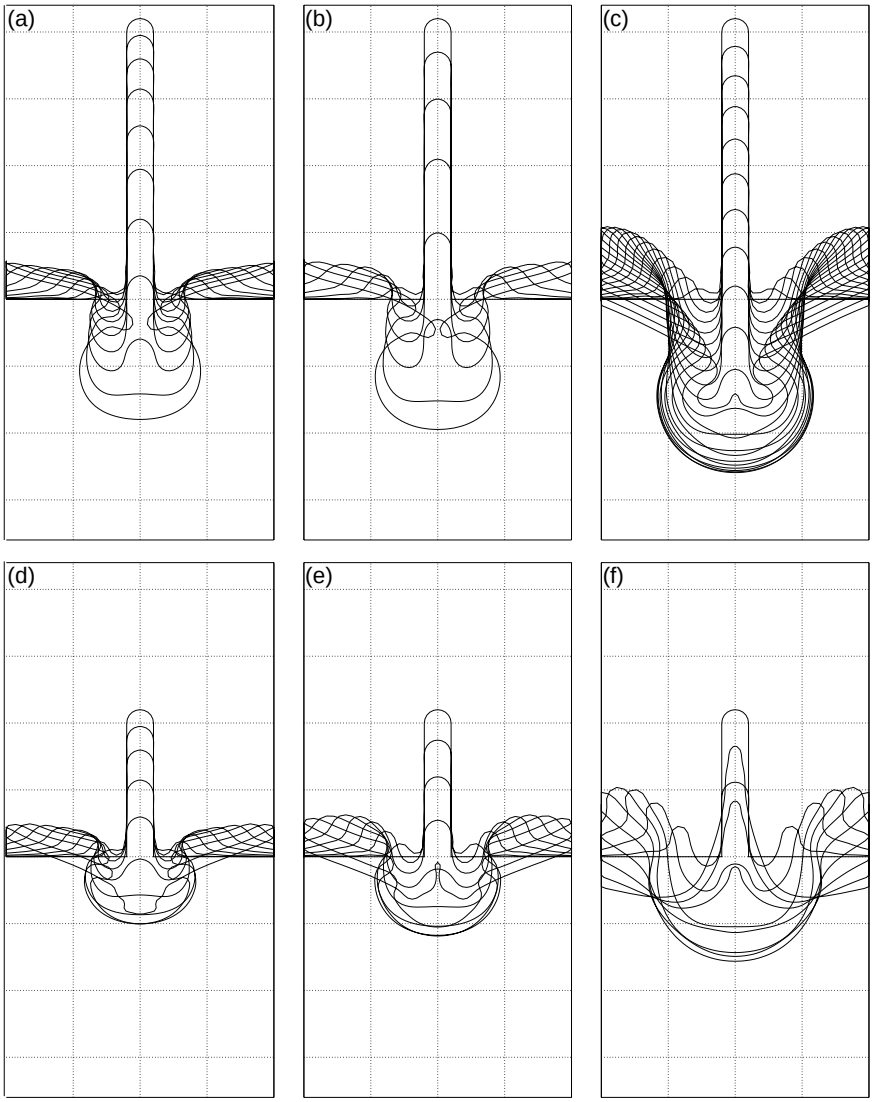

Figure 11. Successive free surface configurations due to the impact of a two-dimensional jet with aspect ratio 20 (top row) and 10. The Froude number equals 2 for (*a*) and (*d*), 8 for (*b*) and (*e*) and 32 for (*c*) and (*f*). Successive contours are separated by 1 dimensionless time unit in (*a*) and (*d*), 5 units in (*f*) and 2 units in the other cases. The last contours shown are, in alphabetical order, at times 10, 14, 44, 10, 20 and 50. In all cases the dashed squares sides equal 5 dimensionless units.

tends to produce an upward moving jet that escapes from the cavity before the inward motion of the side walls can entrap a bubble, as more clearly shown in the last two examples of the following figure. An analogous phenomenon taking place in the trough between two colliding surface waves was described by Peregrine and co-workers (Cooker & Peregrine 1990; Peregrine & Prentice 1994) as 'flip through'. The result of the competition between the inward motion of the side walls and the upward motion of the cavity bottom—that plays a central role in all the cases considered

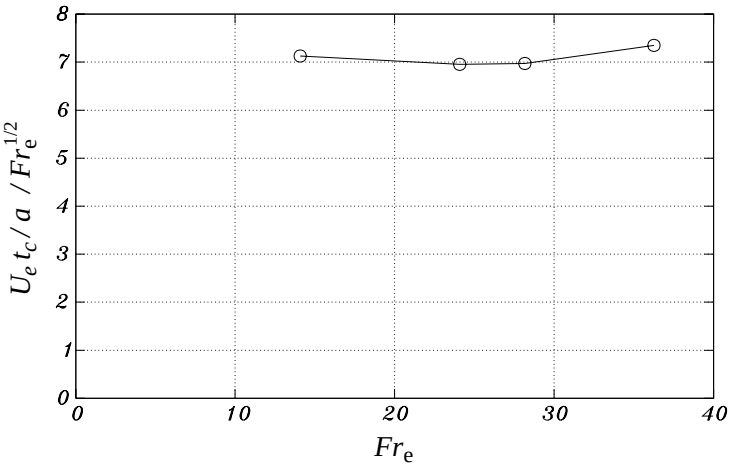

Figure 12. Ratio of predicted, equation (3.10), and numerically computed closing time for two-dimensional cavities.

here—depends on the length of the impacting jet and the Froude number. The last example shown in figure 10 is very close to the borderline between bubble entrapment and the escaping of the upward jet. Only a very small bubble would be entrapped in this case, and no bubble at all for a slightly higher value of Fr or shorter jet.

Numerical results for the two-dimensional case similar to those given in figure 10 are shown in figure 11 for aspect ratios of 20 and 10. Upon comparison with the axisymmetric case it is apparent that air entrapment is a less likely event in two dimensions, chiefly because the crater tends to be much broader.

We can extend to this two-dimensional geometry an argument that we have used earlier in the axisymmetric case to scale the closure time (Oğuz *et al.* 1995). We assume that the time necessary for the closure of the cavity at a depth z can be written as

$$t_c(z) = \frac{z}{\frac{1}{2}U_e} + c\sqrt{\frac{a\left(\frac{1}{2}U_e t_c - z\right)}{gz}}. \tag{3.8}$$

The first term is the time required for the cavity, that proceeds downward with an average velocity $\frac{1}{2}U_e$ as argued before, to reach depth z. The second one is the ratio of the cavity width estimated from (3.5), at a distance $\frac{1}{2}U_e t_c - z$ from its lowest point, to a closure velocity estimated in terms of the hydrostatic head, $\sqrt{gz}$. The undetermined constant c is expected to be of order one. The minimum of t_c over z should approximate the actual closing time and depth. Upon taking the derivative of (3.8) and setting to zero we find the depth D of the closure to be

$$D/a = \tfrac{1}{2}c\, Fr_e^{1/2}, \tag{3.9}$$

from which, upon substituting into (3.8), we find the dimensionless closing time

$$U_e t_c/a = \tfrac{3}{2}c\, Fr_e^{1/2}\,. \tag{3.10}$$

The prediction (3.10) is compared with some numerical results in figure 12, where it is seen to be in good agreement with them for $c \simeq 4.67$. Following the same argument along the lines used in the three-dimensional case (Oğuz *et al.* 1995), one can derive estimates for the volume of the entrapped bubble. Unlike the three-dimensional case,

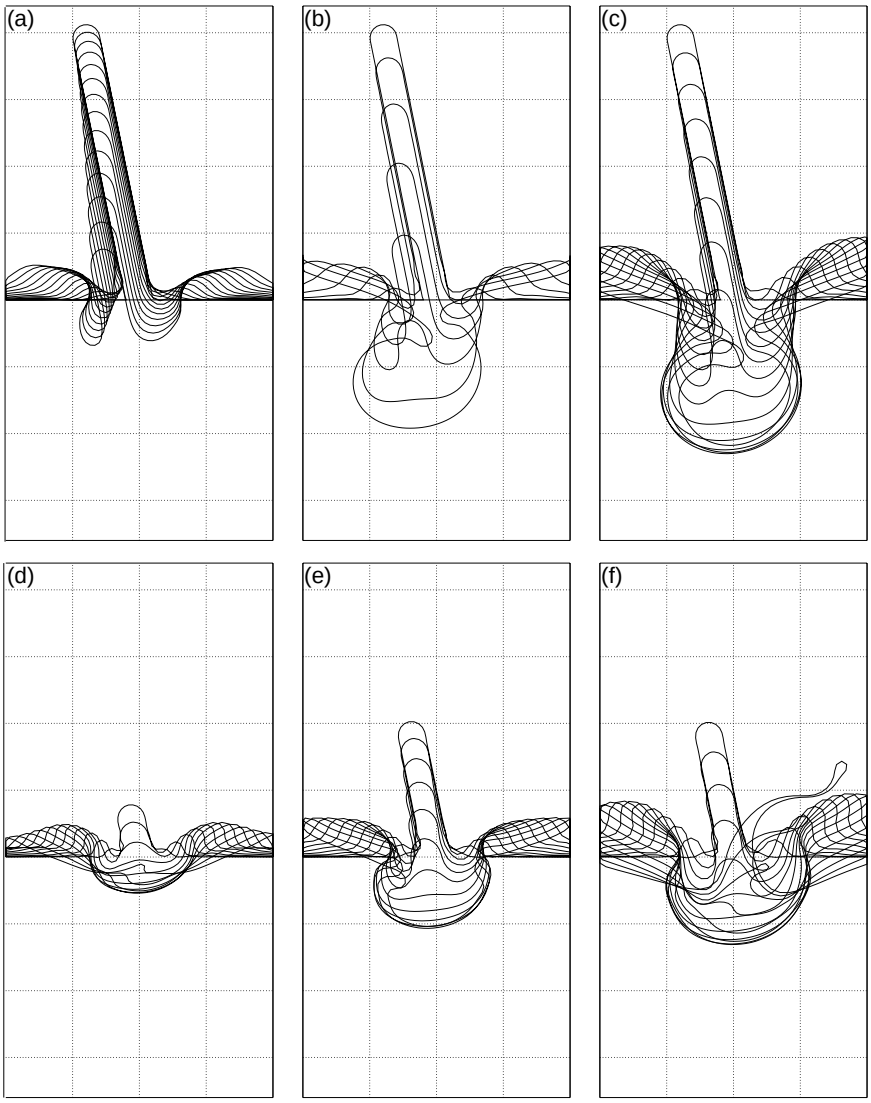

Figure 13. Successive free surface configurations due to the impact of a two-dimensional jet with aspect ratio $h = 20$ (top row), 5 ((d)) and 10 ((e), (f)), and an inclination of 11.46°. The Froude number equals 2.04 in (a), 4.08 in (b), (d) and (e) and 16.3 in (c), (f). Successive contours are separated by 0.5 dimensionless time units in (a), 1 unit in (d), (e) and 2 units in (b), (c) and (f). The last contours shown are, in alphabetical order, at times 6.5, 14, 30, 11.9, 12.6 and 32.7. In all cases the dashed squares sides equal 5 dimensionless units.

however, the result is not in very good agreement with the computations. It may also be noted that, as in our earlier work on the axisymmetric case, the preceding argument has been cast in terms of the energy-based velocity and Froude number. The use of these quantities gives a much better fit than the corresponding ones based on the velocity at impact.

One would expect that the approach just explained could be successfully applied to the overpressure model of the previous section. For the axially symmetric case the result is that both the closure time and the entrapped cavity volume should

scale proportionally to $Fr^{1/3}$. As we have seen, this prediction is at variance with the numerical results for both geometries. Since, as we have just mentioned, a successful scaling on the basis of this argument seems to require the use of Fr_e, rather than Fr, an (admittedly somewhat shaky) explanation of this surprising conclusion might be that the Froude numbers considered before are not sufficiently large for the argument to apply.

The two-dimensional case lends itself readily to the simulation of non-normal impacts. We show some results for an impact angle of 0.2 rad (11.46°) and $h = 20$, 5 and 10 in figure 13. The bubbles entrapped in the cases of figure 13*b* and *c* look very much like what one would expect from the analogous normal-impact cases shown in figure 11*a* and *b*. The smallest Froude number case in figure 13, case *a* shows a different mode of air entrainment with the cavity 'capped' by one side of the incoming jet. One can expect that this process would be very common for greater angles of impact due to geometrical factors. The last example, figure 13*f*, features a prominent thin jet oppositely directed with respect to the original one.

4. Conclusions

In his study entitled 'The fascination of fluid mechanics' published in *J. Fluid Mech.* (25th Anniversary volume), Professor Peregrine devoted more than two thirds of his paper to splashes (Peregrine 1981). The phenomena that we have considered here are intimately related to those studied by him and are perhaps no less fascinating. But in addition to their intrinsic fluid dynamical interest, such liquid–liquid impact events are of fundamental importance as they lie at the root of air entrainment processes in low-viscosity liquids. With respect to the heyday of free-streamline theory in the central decades of this century, when several of the phenomena discussed here were first studied, we enjoy the advantage of powerful computers and numerical techniques. Nevertheless, such flows still present considerable challenges, of which the unresolved issues that we have encountered above are but a few examples.

Before closing, it is necessary to at least mention another very important, and little understood, matter that has been tacitly avoided so far. We refer to the phenomena occurring at the moment at which the initial contact between two disjoint liquid surfaces is established. We have sidestepped this difficulty by starting all of our calculations with the liquids already in contact. A preliminary discussion of the problem was given in an earlier paper (Oğuz & Prosperetti 1989) where it was shown that, most likely, many small bubbles are entrapped in the region where contact is established. In part, their formation is the consequence of thermodynamic non-equilibrium phenomena and hence cannot be followed in a deterministic fluid dynamic calculation with a practical time step. For this reason, it appears necessary to somehow develop a computational approach capable of dealing with this phase of the motion in an artificial way without adversely affecting the subsequent simulation. Some progress in this direction has been made by Best (1993) and by Zhang *et al.* (1993), but it is fair to say that no widely accepted procedure has emerged from these initial attempts.

In conclusion, we mention a possible implication of our results in a very different branch of Science. There is convincing proof that a small fraction of the meteorites found on Earth originate from Mars and the Moon (Gladman *et al.* 1996). The mechanism hypothesized to explain this surprising fact is that this material was ejected from the parent celestial body by the impact of a larger meteorite and then accel-

erated past the escape velocity by the high-velocity vapour plumes formed in the course of this catastrophic event. The quantitative confirmation of this hypothesis rests, at least in part, on two-dimensional numerical simulations of impacts (O'Keefe & Ahrens 1986) that, as the previous calculations show, tend to considerably overestimate the magnitude and velocity of the splash created by the impact. If less mass rises over the surface of the planet at a smaller velocity and a lower elevation than is estimated on the basis of such calculations, it is less likely that it be accelerated to the required speeds. It may therefore be necessary to confirm the two-dimensional estimates by more precise three-dimensional calculations.

Support by the Office of Naval Research is gratefully acknowledged. H.N.O. has been supported in part also by NSF under CTS 9318724.

References

Best, J. P. 1993 The formation of toroidal bubbles upon the collapse of transient cavities. *J. Fluid Mech.* **251**, 79–107.

Biń, A. K. 1993 Gas entrainment by plunging liquid jets. *Chem. Engng Sci.* **48**, 3585–3630.

Birkhoff, G. & Caywood, T. E. 1949 Fluid flow patterns. *J. Appl. Phys.* **20**, 646–659.

Birkhoff, G. & Zarantonello, E. H. 1957 *Jets, wakes, and cavities.* New York: Academic.

Cooker, M. J. & Peregrine, D. H. 1990 Violent water motion at breaking-wave impact. In *Proc. 22nd Int. Conf. on Coastal Engineering*, vol. 1, pp. 164–176. Delft: ASCE.

Gilbarg, D. 1960 Jets and cavities. In *Encyclopedia of physics* (ed. S. Flügge & C. Truesdell), pp. 311–445. Berlin: Springer.

Gladman, B. J., Burns, J. A., Duncan, M., Lee, P. & Levison, A. F. 1996 The exchange of impact ejecta between terrestrial planets. *Science* **271**, 1387–1392.

Lin, T. J. & Donnelly, H. G. 1966 Gas bubble entrainment by plunging laminar liquid jets. *A. I. Ch. E. Jl* **12**, 563–571.

Milne-Thomson, L. M. 1960 *Theoretical hydrodynamics*, IVth edn. New York: MacMillan.

Oğuz, H. N. & Prosperetti, A. 1990 Bubble entrainment by the impact of drops on liquid surfaces. *J. Fluid Mech.* **219**, 143–179.

Oğuz, H. N. & Prosperetti, A. 1990 Surface tension effects in the contact of liquid surfaces. *J. Fluid Mech.* **203**, 149–171.

Oğuz, H. N. & Prosperetti, A. 1991 Numerical calculation of the underwater noise of rain. *J. Fluid Mech.* **228**, 417–442.

Oğuz, H. N. & Prosperetti, A. 1993 Dynamics of bubble growth and detachment from a needle. *J. Fluid Mech.* **257**, 111–145.

Oğuz, H. N. & Prosperetti, A. 1994 Mechanics of air entrainment by a falling liquid. In *Aeration technology* (ed. R. E. A. Arndt & A. Prosperetti), pp. 13–20. New York: American Society of Mechanical Engineers.

Oğuz, H. N., Prosperetti, A. & Kolaini, A. R. 1995 Air entrapment by a falling water mass. *J. Fluid Mech.* **294**, 181–207.

O.Keefe, J. D. & Ahrens, T. J. 1986 Oblique impact: a process for obtaining meteorite samples from other planets. *Science* **234**, 346–349.

Peregrine, D. H. 1981 The fascination of fluid mechanics. *J. Fluid Mech.* **106**, 59–80.

Peregrine, D. H. & Prentice, P. R. 1994 Jet formation at a free surface. In *Bubble dynamics and interface phenomena* (ed. J. R. Blake, J. M. Boulton-Stone & N. H. Thomas), pp. 397–404. Dordrecht: Kluwer.

Sene, K. J. 1988 Air entrainment by plunging jets. *Chem. Engng Sci.* **43**, 2615–2623.

Zhang, S. G., Duncan, J. H. & Chahine, G. L. 1993 The final stage of the collapse of a cavitation bubble near a wall. *J. Fluid Mech.* **257**, 147–181.